

Direct Visualization of Independent Ta Centers supported on 2D TiO₂ nanosheets

Zhenyu Bo¹, Nick Thornburg², Lingxuan Peng¹, Jose Julio Gutierrez Moreno³, Michael Nolan³, Laurence D. Marks¹, Justin M. Notestein^{2*}

1. Department of Materials Science and Engineering, Northwestern University, Evanston, IL, 60208
 2. Department of Chemical and Biological Engineering, Northwestern University, Evanston, IL, 60208
 3. Tyndall National Institute, University College Cork, Lee Maltings, Dyke Parade, Cork, Ireland
- * Corresponding author email: j-notestein@northwestern.edu

ABSTRACT

Highly-dispersed, supported oxides are ubiquitous solid catalysts, but they can be challenging to characterize with atomic precision. Here it is shown that crystalline anatase TiO₂ nanosheets (~5 nm thick) are ideal supports for imaging highly-dispersed active sites. Ta cations are deposited by several routes, and high-resolution high angle annular dark-field (HAADF) scanning transmission electron microscopy (STEM) is used to determine the location of Ta with respect to the TiO₂ lattice and to quantify Ta-Ta distances. In the best case, it is shown that >80% of Ta atoms are isolated from one another, whereas other techniques are blind to this critical catalytic property or give only qualitative estimates. TiO₂ nanosheets may prove to be a useful platform for other types of catalysis studies.

KEYWORDS

HAADF STEM; supported catalysts; oxides; microscopy; single atom catalysts

1
2
3 Heterogeneous catalysts are solid materials that catalyze reactions in the gas or liquid
4 phase, and are essential in chemicals manufacturing, fuels production and emissions control.^{1,2}
5 They take a variety of forms including supported metal nanoparticles such as Pt/Al₂O₃ for
6 hydrogenation/dehydrogenation or combustion,³ bulk oxides such as the complex MoVTaNbO
7 materials used in ammoxidation,⁴ or supported metal oxides such as TiO_x/SiO₂ and VO_x/TiO₂.^{5,}
8
9
10
11
12
13
14
15
16
17
18
19
20
21
22
23
24
25
26
27
28
29
30
31
32
33
34
35
36
37
38
39
40
41
42
43
44
45
46
47
48
49
50
51
52
53
54
55
56
57
58
59
60
6 This last category is frequently used in reactions such as the selective oxidation of alcohols
and alkenes, emissions control, and photocatalysis.⁷⁻¹⁰

The reactivity of any heterogeneous catalyst is dependent on the number of the active atoms (e.g. Ti atoms in TiO_x/SiO₂ catalysts) that are accessible to the reactants.^{6, 11, 12} To keep this value as high as possible, catalysts are typically synthesized to be as dispersed as possible while retaining their active form, giving oxide domains that are ideally present as single cations on the support, small clusters, or monolayers. In addition, supported oxides are also well-known to be 'structure-sensitive', in that their precise atomic connectivity to other active atoms and to the support has a large impact on catalytic rates and selectivities.¹³⁻¹⁶

Therefore, the catalysis community is continuously looking for methods to control the chemical environment and the dispersion of active sites during the synthesis of supported metal oxide catalysts. These methods can include the use of bulky or well-defined precursors to enforce site-isolation,^{17, 18} multinuclear precursors to create small clusters,¹⁹⁻²¹ thermolytic molecular precursors,^{22, 23} substituted silsesquioxanes,^{23, 24} atomic layer deposition,²⁵⁻²⁷ and engineered supports,²⁸⁻³⁰ among many other approaches.

Beyond the synthesis, a significant challenge in supported oxides of all types is characterizing them with atomic precision. Historically, characterization of the active sites of supported oxide catalysts has been via probe reactions and via X-ray absorption, UV-visible, NMR, vibrational, and other spectroscopies. However, these techniques all give local properties of the probed atom, and are also averaged over the whole sample, making it

1
2
3 challenging to tease out some of the finer details of synthesis-structure-function relationships,
4
5 such as the distribution of atoms across a surface. Finally, chemical site counting methods can
6
7 provide distributions of the properties of active sites,^{31, 32} but do not necessarily provide
8
9 structural information.
10

11
12 Significant advances have been made in recent years for the direct, atomic-level
13
14 visualization of supported catalyst active sites by electron microscopy, even as the active sites
15
16 themselves trend towards single-atom dimensions.^{33, 34} However, there remain several
17
18 significant limitations. First, most imaging of single-atom and small cluster catalysts has
19
20 occurred with 3rd row, low-valent, late transition metals (eg. Au, Pt, Ir).³³⁻³⁵ These elements
21
22 provide good Z-contrast and are widely used catalysts. In contrast, supported, high-valent, early
23
24 transition metal cations and oxides have not been the target of these types of imaging studies,
25
26 likely because the 1st row elements are more commonly used in catalysis within these groups.
27
28 Second, zeolites and other crystalline oxides like SrTiO₃ have been preferred for atomic-
29
30 resolution imaging of supported species, in part because of the relative ease of imaging along
31
32 a particle edge on such supports.^{36, 37} It is more challenging to image species with atomic
33
34 resolution on the surface of traditional, high surface areas supports such as Al₂O₃, TiO₂ and
35
36 SiO₂ because of their amorphous or highly faceted surfaces and relatively large primary
37
38 particles. There have been successes using core-shell or very small support oxide particles to
39
40 image and locate single catalyst atoms,^{38, 39} but it remains very challenging to focus highly
41
42 converged electron beams on more than a small area at a time.
43
44
45
46
47
48

49 In this letter, we report the use of 2D TiO₂ nanosheets (nsTiO₂) as nearly ideal support
50
51 materials for the direct visualization of highly-dispersed catalysts across large particle surface
52
53 areas. Here, we demonstrate its utility for tantalum oxides (TaO_x/TiO₂) to address the dearth
54
55 of imaging of supported, high-valent, early transition metal cations, but these supports should
56
57 be generally applicable for imaging supported catalysts. The use of thin (~5 nm), flat, anatase
58
59
60

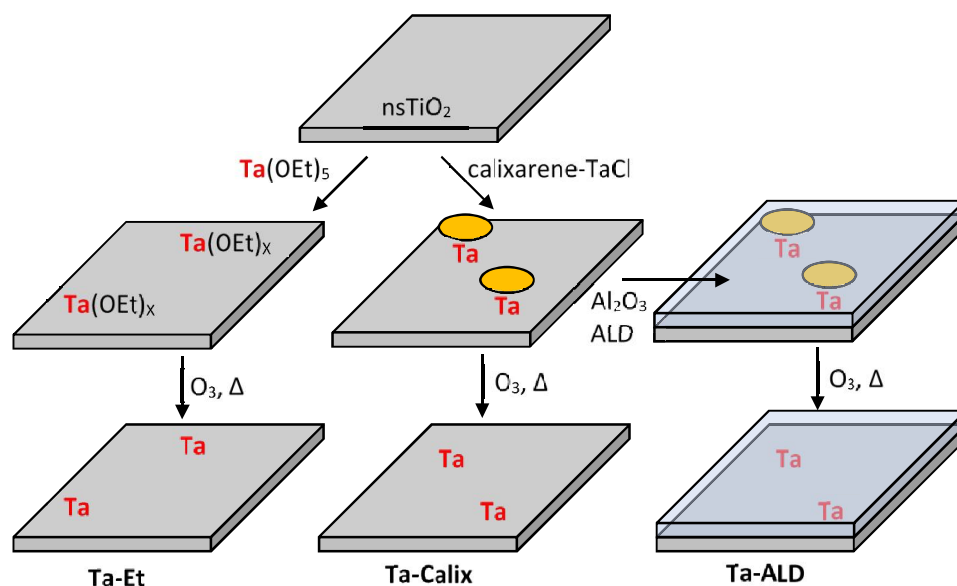
1
2
3 TiO₂ nanosheets instead of traditional oxide particles makes it possible to keep the entire
4 surface in focus during High-Resolution High Angle Annular Dark-Field (HAADF) imaging,
5 rather than very small regions on a particle edge, as is typical for conventional supports.
6
7 Moreover, in contrast to prior examples of STEM,⁴⁰ STM,^{41, 42} or atom-probe tomography,⁴³
8 high surface area powders are used here, permitting bulk characterization tools to be used on
9 the same material with no special modifications. Second- and third-row highly dispersed metal
10 oxides are less commonly used than their first-row counterparts, but have recently gained
11 attention for having comparable, or in many cases greater, activity or selectivity in a variety of
12 thermochemical transformations.^{7, 15} TaOx-based materials have been shown to be interesting
13 in a variety of selective oxidation reactions,⁴⁴⁻⁴⁶ and Ta-TiO₂ specifically is of interest as an
14 acid catalyst⁴⁷ and for its photocatalytic properties.⁴⁸⁻⁵⁰

15
16
17
18
19
20
21
22
23
24
25
26
27
28
29
30
31
32
33
34
35
36
37
38
39
40
41
42
43
44
45
46
47
48
49
50
51
52
53
54
55
56
57
58
59
60
The images collected here provide direct evidence for single-atom dispersion and provide the distribution of Ta-Ta nearest-neighbor distances over a wide area, giving insight into the sensitivity of the TaOx structure on the Ta precursor used for synthesis. It also gives insight into the effects of post-synthetic modifications, such as subsequent atomic layer deposition of an additional oxide. Precursor and post-synthesis modification have both been shown to strongly influence the catalyst activity and stability,^{25, 30, 51} but as mentioned above, direct connections to surface speciation have remained elusive.

15
16
17
18
19
20
21
22
23
24
25
26
27
28
29
30
31
32
33
34
35
36
37
38
39
40
41
42
43
44
45
46
47
48
49
50
51
52
53
54
55
56
57
58
59
60
TiO₂ nanosheets (nsTiO₂) were synthesized using titanium butoxide and hydrofluoric acid under autoclave conditions following previously reported procedures.⁵² The N₂ physisorption specific surface area measured (Supporting Information Figure S1) by the BET method is 145 m²/g. These materials consist of platelets with particle dimensions of length and width below 100 nm and thickness below 10 nm (SI Figure S2) Typical particles have length and width of ~60 nm and a thickness of ~ 5 nm. These materials have pure anatase phase, with X-ray diffraction peaks corresponding to the (101), (004), (200), (105) and (211) crystal planes

1
2
3 (SI Figure S3).⁵³ The particles are not annealed, and the large faces are unreconstructed and
4 [001]-terminated.⁵² The particles are flat for imaging over extended distances, but the faces are
5 not atomically smooth and are expected to contain the types of surface defects found in other
6 TiO₂ materials.
7
8
9
10
11

12 To deposit Ta atoms, (illustrated in Scheme 1), nsTiO₂ was dispersed in a toluene
13 solution containing either calixarene-TaCl (30mM, 40mL, ultimately giving material **Ta-**
14 **Calix**)⁵⁴ as a representative bulky precursor previously shown to help enforce site-isolation on
15 silica, or Ta(OEt)₅ (Sigma-Aldrich, 15mM, 10mL, ultimately giving materials **Ta-Et**) and the
16 solution was heated to reflux for 24 h. The modified nsTiO₂ was washed with anhydrous
17 toluene and dried under dynamic vacuum at room temperature. This procedure grafts the Ta
18 atoms at a surface density of ~0.3 Ta nm⁻², or 70 μmol Ta g⁻¹ as determined by
19 thermogravimetric analysis (to measure calixarene ligand content, SI Figure S4) and ICP-OES
20 (Ta content). This loading was chosen because it is approximately the geometrical limit
21 resulting from the large calixarene ligand.²⁵ Some samples of as-synthesized **Ta-Calix** were
22 coated with <1 nm Al₂O₃ using atomic layer deposition (ALD) of five alternating cycles of
23 Al(CH₃)₃ and H₂O,²⁵ ultimately leading to material **Ta-ALD**. Finally, all samples were treated
24 in flowing O₃ at 110°C to remove any residual organic ligands. In addition to electron
25 microscopy, samples were also characterized by X-ray diffraction (XRD) and X-ray
26 photoelectron (XPS), diffuse reflectance UV-visible (DRUV-vis), and Raman spectroscopies.
27
28
29
30
31
32
33
34
35
36
37
38
39
40
41
42
43
44
45
46
47 See SI for full procedures.
48
49
50
51
52
53
54
55
56
57
58
59
60



Scheme 1. Modification of anatase 001-terminated TiO_2 nanosheets (nsTiO_2) with Ta and with an Al_2O_3 overcoat

HAADF imaging was completed using a JEOL JEM-ARM200CF aberration-corrected scanning transmission electron microscope. To prepare the sample for imaging, ethanol suspensions of samples were drop-cast onto TEM grids and air-dried. The HAADF images were acquired using a probe of ~ 0.078 nm, an emission current of $15 \mu\text{A}$ and a beam current of $\sim 19\text{pA}$ with a $40 \mu\text{m}$ condenser lens aperture. The collection angle of the HAADF was greater than 80 degrees. Ta atom nearest neighbor distances (NND) were calculated using Image J software.

Conventional spectroscopies and other characterization tools are often limited in the information they can provide for mixed or supported oxides, as they give ensemble averages of the materials. XRD after Ta deposition or after ALD (SI Figure S3) shows no changes or additional features. This indicates that neither did a TaO_x crystal phase form on top of the nsTiO_2 nor did Ta insert into the TiO_2 lattice to any significant extent, but it provides no information on the actual TaO_x structure adopted. XPS (SI Figure S5) shows binding energy peaks at 458.6 eV and 464.5 eV in the Ti 2p region and at 530.5 eV in the O 1s region, which are typical of Ti^{4+} and oxygen ions in metal oxides.⁵³ The Ta 4f peaks around 26 eV and 28 eV

1
2
3 confirm the presence of Ta with high oxidation state in the Ta-containing samples.^{55, 56, 57} The
4 absence of observable features near 855 cm^{-1} in the Raman spectrum could indicate the absence
5 of Ta-O-Ta bonds that would be found in larger clusters.⁵⁸ However, as is often the case with
6 supported oxide catalysts, stronger conclusions are precluded by the relatively low loadings of
7 Ta and the strong contribution from nsTiO₂ itself. Likewise, DRUV-vis can be a useful tool for
8 characterizing supported oxides,^{6, 7} but here cannot distinguish the Ta-containing materials
9 from the parent nsTiO₂ (SI Figure S7). Overall, XRD, XPS and Raman studies confirm the
10 presence of small amounts of highly dispersed Ta oxide on anatase nsTiO₂ but cannot provide
11 further details.
12
13
14
15
16
17
18
19
20
21
22

23
24 Therefore, high-resolution HAADF-STEM images were acquired to enable direct
25 observation of the distribution of Ta atoms on the TiO₂ surface with atomic resolution. Figure
26 1a) shows the structure of **Ta-Et** taken along the [001] direction of the nsTiO₂ crystallite. The
27 image clearly demonstrates that the Ta atoms are located on top of the Ti-O columns, and there
28 were no Ta atoms located between columns. This alignment requires that the Ta atoms were
29 present either directly above the Ti lattice sites, or as substitutions for Ti atoms within the
30 lattice or at the surface. Because of the synthesis method and the mild post-synthesis treatments,
31 it is most likely that Ta grafts directly above the Ti atoms. Density functional theory (see SI
32 for details) confirms that, regardless of the extents of Ta atom hydration and surface
33 hydroxylation, the stable configuration places Ta atoms directly above a Ti atom column, as
34 illustrated in Figure 1b) and Figure 1c). We note that the Ta atoms occupy different
35 crystallographic positions depending on the state of hydration, although we cannot verify this
36 from the microscopy. The circles in Figure 1a) highlight some of the many isolated Ta atoms
37 (no Ta atoms at the neighboring lattice position) in this sample. The squares in Figure 1 show
38 some potential pairs or oligomers of Ta atoms at adjacent sites.
39
40
41
42
43
44
45
46
47
48
49
50
51
52
53
54
55
56
57
58
59
60

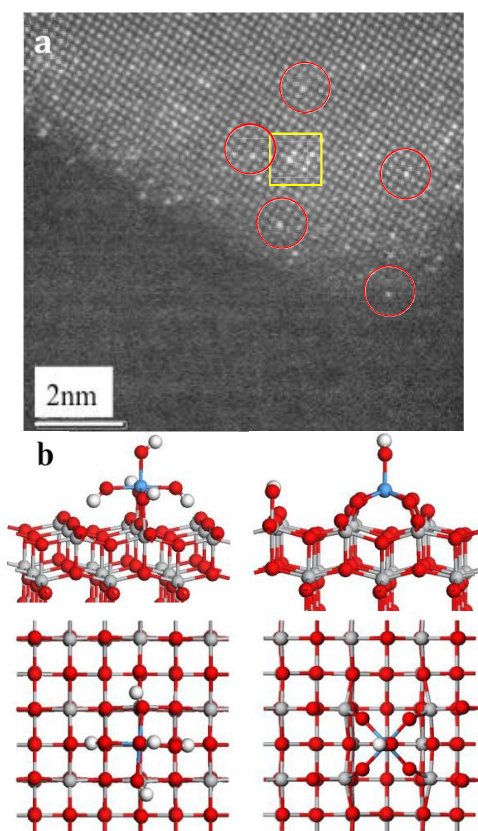
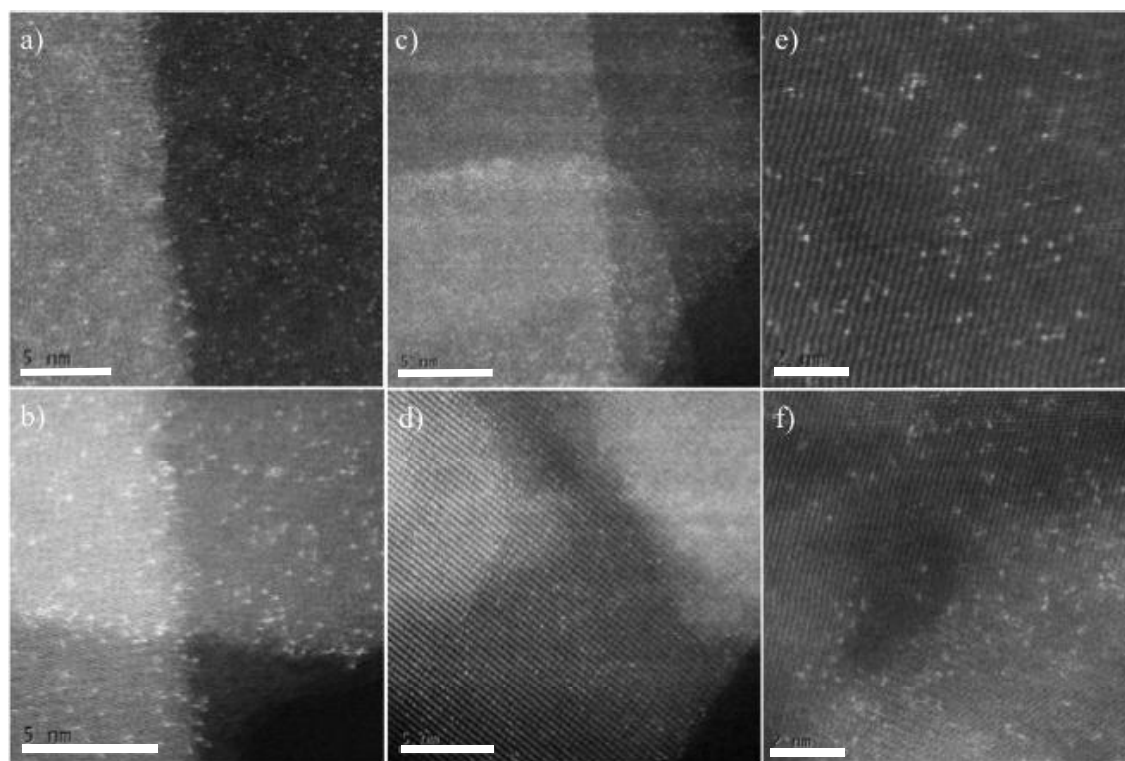


Figure 1. a) High-resolution HAADF-STEM image of sample **Ta-Et** acquired along the [001] direction of the TiO₂ support. A median filter with a window of size 2 was applied to this image. The unprocessed image is given in SI Figure S8. The bright dots are individual Ta atoms. Red circles highlight isolated Ta atoms and the yellow square highlights potential regions where Ta atoms are found in adjacent sites, b) optimized structures of Ta⁵⁺ supported on a TiO₂ anatase (001) surface generated using density functional theory modeling showing alignment of Ta with Ti columns, whether fully hydrated (left) or dehydrated (right); see SI for discussion. Red = O, gray = Ti, blue = Ta, white = H.

Next, the unique ability to locate Ta atoms over longer distances on nsTiO₂ is used to map out Ta-Ta distances for the materials. Figure 2 shows a representative set of atomic resolution HAADF-STEM images of **Ta-Et**, **Ta-Calix** and **Ta-ALD** taken in plan-view to obtain information about Ta-Ta spacing. Because of the planar supports, single images provide information representative of the entire sample. For example, Figure 2d shows 186 atoms over approximately 350 nm² of imaged area (700 nm² of TiO₂ surface). This gives 3.7 nm² Ta⁻¹, in good agreement with the specific surface area of the nsTiO₂ divided by the total amount of Ta

1
2
3 grafted ($3.3 \text{ nm}^2 \text{ Ta}^{-1}$). From visual inspection alone, the two Ta precursors do not produce
4
5 markedly different Ta distributions on the surface, with many isolated atoms in both cases. In
6
7 addition, the Ta distribution is not apparently changed by Al_2O_3 overcoating by ALD. The
8
9 ALD process utilizes the very reactive molecule $\text{Al}(\text{CH}_3)_3$ and generates water vapor at
10
11 moderate temperatures, and it was initially suspected that the process might significantly
12
13 rearrange the surface TaO_x . We also note that while the nsTiO_2 supports can be damaged by
14
15 long electron beam exposures, the Ta remain as single atoms, with no obvious changes to their
16
17 orientation with respect to the TiO_2 surface. (Figure S9a and b) This contrasts with control
18
19 materials such as Ta on silica nanospheres, in which the Ta is challenging to visualize initially
20
21 then obviously aggregates during microscopy. (Figure S9c and d)
22
23
24
25
26
27
28



54
55 **Figure 2.** Representative high resolution HAADF-STEM images of a,b) **Ta-Calix**, c,d) **Ta-Et**,
56 e,f) **Ta-ALD**. Scale bars in a-d are 5 nm. Scale bars in e and f are 2 nm.
57
58
59
60

These images enabled by the extended, flat surface of nsTiO₂ allows for statistically meaningful estimates (N = 134-186 Ta atoms) of the distribution of supported Ta atoms from a small number of images. The observed nearest neighbor distances (NND) are calculated for all visible Ta atoms in Figure 2 (see also SI Figure S10). The median NND for materials **Ta-Et**, **Ta-Calix**, and **Ta-ALD** are 0.5, 0.7, and 0.5 nm. From the 3.3 nm² Ta⁻¹ average loading, Ta perfectly dispersed on the surface would have an apparent Ta-Ta separation of 0.9 nm. We also quantitatively estimate the fraction of Ta atoms that are 'isolated' from another, by placing a cutoff Ta-Ta separation of >0.4 nm from the nearest neighbor, approximately the Ta-O-Ta distance in Ta₂O₅.⁵⁹ The cumulative frequency distributions in Figure 3 show that for all materials, >60% of Ta atoms are isolated from each other, with potentially >80% of the Ta atoms being isolated in the case of **Ta-Calix**, which is derived from the bulky precursor. It is emphasized that these estimates are conservative. Because the imaging technique visualizes all Ta atoms in a 2D space, Ta atoms sitting on the other side of the TiO₂ nanosheets were also imaged, thus increasing the apparent Ta surface density.

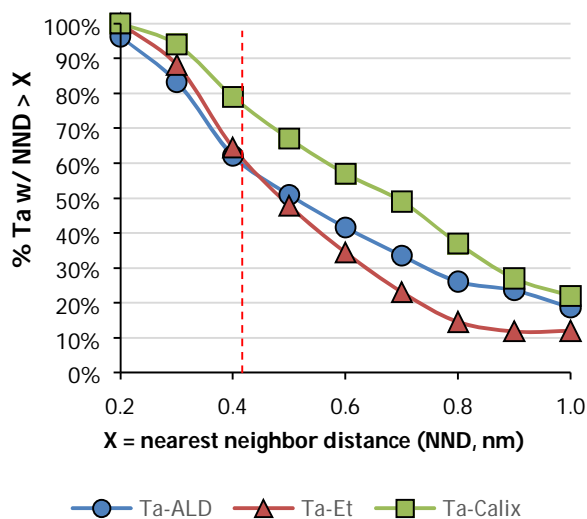


Figure 3. Cumulative frequency plot of nearest neighbor distance (NND, Ta to Ta distance in nm) for samples **Ta-Et** (186 atoms counted), **Ta-Calix** (134 atoms counted) and **Ta-ALD** (161 atoms counted). Ta to Ta distances ≤ 0.4 nm, indicated by the red line, might indicate the formation of Ta-O-Ta bonds.

1
2
3 'Isolated' sites have long been argued from spectroscopy to be the most active sites in
4
5 a number of reactions,^{35,60} and many synthetic methods, including the use of bulky ligands such
6
7 as calixarene,^{54,25} have been specifically developed to bias the system towards a preponderance
8
9 of these sites. For the first time, we have directly demonstrated the validity of these claims
10
11 from HAADF-STEM imaging. Recalling that **Ta-ALD** is derived from the same precursor
12
13 material as **Ta-Calix**, the full analysis of the Ta-Ta distances also shows that the conditions of
14
15 the ALD indeed cause some rearrangement and aggregation of TaOx, even if the aggregation
16
17 is not severe enough to be observed by bulk techniques. In conclusion, we have demonstrated
18
19 the use of TiO₂ nanosheets as excellent 2D supports for high resolution STEM imaging of
20
21 highly-dispersed, supported catalysts and quantification of atom-atom distance distributions.
22
23 We are currently working to apply this technique to other catalytic metals and systems.
24
25
26
27
28
29

30 **ASSOCIATED CONTENT**

31
32
33 **Supporting Information.** Materials synthesis procedures; characterization: N₂ physisorption,
34
35 XRD, TGA, XPS, Raman, UV-visible; additional TEM and Ta-Ta distance histograms;
36
37 computational details and results
38
39

40 **Corresponding Author**

41
42
43
44 *Email for J.M.N.: j-notestein@northwestern.edu
45
46

47 **Notes**

48
49 The authors declare no competing financial interest.
50
51

52 **Acknowledgements**

53
54
55 This material is based upon work supported by the U.S. Department of Energy, Office of
56
57 Science, Office of Basic Energy Science, under Award Number DOE DE-FG02-03ER15457
58
59 to the Institute for Catalysis for Energy Processes (ICEP) at Northwestern University. This
60

1
2
3 work was supported by the Materials Research Center (MRSEC) at Northwestern University,
4
5 on grant number DMR-112126. N.E.T. and J.M.N. acknowledge financial support from the
6
7 Dow Chemical Company. This work made use of the EPIC facility of the NUANCE Center at
8
9 Northwestern University, which has received support from the Soft and Hybrid
10
11 Nanotechnology Experimental (SHyNE) Resource (NSF NNCI-1542205); the MRSEC
12
13 program (NSF DMR-112126) at the Materials Research Center; the International Institute for
14
15 Nanotechnology (IIN); the Keck Foundation; and the State of Illinois, through the IIN. This
16
17 work made use of the JEOL JEM-ARM200CF in the Electron Microscopy Service [Research
18
19 Resources Center, University of Illinois at Chicago (UIC)]. JJGM and MN acknowledge
20
21 support from the Irish Environmental Protection Agency UisceSense project (W-2015-MS-21)
22
23 and the SFI-NSF-DEL US Ireland R&D Partnership Program, grant number SFI US/14/e2915
24
25 and access to computational resources through the Irish Center for High End Computing. We
26
27 acknowledge supply of raw materials (TiO₂ nanosheets) by Dr. Kevin Schwartzberg
28
29 (Northwestern University) and atomic layer deposition work by Cassie George (Northwestern
30
31 University).

References

1. Satterfield, C. N., *Heterogeneous Catalysis in Industrial Practice. 2nd Edition.* 1991.
2. Mizuno, N.; Misono, M. *Chem. Rev.* **1998**, *98*, 199-218.
3. Stanislaus, A.; Cooper, B. H. *Catalysis Reviews—Science and Engineering* **1994**, *36*, 75-123.
4. Millet, J.; Roussel, H.; Pigamo, A.; Dubois, J.; Jumas, J. *Appl. Catal. A: Gen.* **2002**, *232*, 77-92.
5. Olthof, B.; Khodakov, A.; Bell, A. T.; Iglesia, E. *J. Phys. Chem. B* **2000**, *104*, 1516-1528.
6. Gao, X.; Wachs, I. E. *Catal. Today* **1999**, *51*, 233-254.
7. Thornburg, N. E.; Thompson, A. B.; Notestein, J. M. *ACS Catal.* **2015**, *5*, 5077-5088.
8. Wachs, I. E. *Dalton Trans.* **2013**, *42*, 11762-11769.
9. Mallat, T.; Baiker, A. *Chem. Rev.* **2004**, *104*, 3037-3058.
10. Clerici, M.; Bellussi, G.; Romano, U. *J. Catal.* **1991**, *129*, 159-167.
11. Xu, Z.; Xiao, F.-S.; Purnell, S.; Alexeev, O.; Kawi, S.; Deutsch, S.; Gates, B. *Nature* **1994**, *372*, 346-348.
12. Van Santen, R. A. *Acc. Chem. Res.* **2008**, *42*, 57-66.
13. Weckhuysen, B. M.; Keller, D. E. *Catal. Today* **2003**, *78*, 25-46.

14. Grant, J. T.; Carrero, C. A.; Love, A. M.; Verel, R.; Hermans, I. *ACS Catal.* **2015**, *5*, 5787-5793.
15. Onfroy, T.; Clet, G.; Houalla, M. *J. Phys. Chem. B* **2005**, *109*, 14588-14594.
16. Tian, H.; Ross, E. I.; Wachs, I. E. *J. Phys. Chem. B* **2006**, *110*, 9593-9600.
17. Prieto-Centurion, D.; Notestein, J. M. *J. Catal.* **2011**, *279*, 103-110.
18. Jarupatrakorn, J.; Tilley, T. D. *J. Am. Chem. Soc.* **2002**, *124*, 8380-8388.
19. Wegener, S. L.; Marks, T. J.; Stair, P. C. *Acc. Chem. Res.* **2011**, *45*, 206-214.
20. Wegener, S. L.; Kim, H.; Marks, T. J.; Stair, P. C. *J. Phys. Chem. Lett.* **2011**, *2*, 170-175.
21. Hess, C.; Hoefelmeyer, J. D.; Tilley, T. D. *J. Phys. Chem. B* **2004**, *108*, 9703-9709.
22. Furdala, K. L.; Tilley, T. D. *J. Catal.* **2003**, *216*, 265-275.
23. Nozaki, C.; Lugmair, C. G.; Bell, A. T.; Tilley, T. D. *J. Am. Chem. Soc.* **2002**, *124*, 13194-13203.
24. Duchateau, R. *Chem. Rev.* **2002**, *102*, 3525-3542.
25. Canlas, C. P.; Lu, J.; Ray, N. A.; Grosso-Giordano, N. A.; Lee, S.; Elam, J. W.; Winans, R. E.; Van Duyne, R. P.; Stair, P. C.; Notestein, J. M. *Nature Chem.* **2012**, *4*, 1030-6.
26. Liu, R.; Lin, Y.; Chou, L. Y.; Sheehan, S. W.; He, W.; Zhang, F.; Hou, H. J.; Wang, D. *Angew. Chem.* **2011**, *123*, 519-522.
27. Herrera, J. E.; Kwak, J. H.; Hu, J. Z.; Wang, Y.; Peden, C. H. *Top. Catal.* **2006**, *39*, 245-255.
28. Thomas, J. M.; Hernandez-Garrido, J. C.; Raja, R.; Bell, R. G. *Phys. Chem. Chem. Phys.* **2009**, *11*, 2799-2825.
29. Chal, R.; Gérardin, C.; Bulut, M.; Van Donk, S. *ChemCatChem* **2011**, *3*, 67-81.
30. Gao, X.; Wachs, I. E. *Top. Catal.* **2002**, *18*, 243-250.
31. Eaton, T. R.; Boston, A. M.; Thompson, A. B.; Gray, K. A.; Notestein, J. M. *ChemCatChem* **2014**, *6*, 3215-3222.
32. Eaton, T. R.; Campos, M. P.; Gray, K. A.; Notestein, J. M. *J. Catal.* **2014**, *309*, 156-165.
33. Ding, K.; Gulec, A.; Johnson, A. M.; Schweitzer, N. M.; Stucky, G. D.; Marks, L. D.; Stair, P. C. *Science* **2015**, *350*, 189-192.
34. Fu, Q.; Saltsburg, H.; Flytzani-Stephanopoulos, M. *Science* **2003**, *301*, 935-938.
35. Kistler, J. D.; Chotigkrai, N.; Xu, P.; Enderle, B.; Praserthdam, P.; Chen, C. Y.; Browning, N. D.; Gates, B. C. *Angew. Chem.* **2014**, *126*, 9050-9053.
36. Flytzani-Stephanopoulos, M.; Gates, B. C. *Ann. Rev. Chem. Biomol. Eng.* **2012**, *3*, 545-574.
37. Chen, B.-R.; Crosby, L. A.; George, C.; Kennedy, R. M.; Schweitzer, N. M.; Wen, J.; Van Duyne, R. P.; Stair, P. C.; Poepelmeier, K. R.; Marks, L. D.; Bedzyk, M. J. *ACS Catal.* **2018**, *8*, 4751-4760.
38. DeRita, L.; Resasco, J.; Dai, S.; Boubnov, A.; Thang, H. V.; Hoffman, A. S.; Ro, I.; Graham, G. W.; Bare, S. R.; Pacchioni, G.; Pan, X.; Christopher, P. *Nature Mater.* **2019**, *18*, 746-751.
39. Lee, B.-H.; Park, S.; Kim, M.; Sinha, A. K.; Lee, S. C.; Jung, E.; Chang, W. J.; Lee, K.-S.; Kim, J. H.; Cho, S.-P.; Kim, H.; Nam, K. T.; Hyeon, T. *Nature Mater.* **2019**, *18*, 620-626.
40. Chang, T.-Y.; Tanaka, Y.; Ishikawa, R.; Toyoura, K.; Matsunaga, K.; Ikuhara, Y.; Shibata, N. *Nano Lett.* **2014**, *14*, 134-138.
41. Fernandez-Garcia, M.; Martinez-Arias, A.; Hanson, J.; Rodriguez, J. *Chem. Rev.* **2004**, *104*, 4063-4104.
42. Bell, A. T. *Science* **2003**, *299*, 1688-1691.
43. Buurmans, I. L.; Weckhuysen, B. M. *Nature Chem.* **2012**, *4*, 873-886.
44. Morlanes, N.; Notestein, J. M. *J. Catal.* **2010**, *275*, 191-201.
45. Nauert, S. L.; Savereide, L.; Notestein, J. M. *ACS Catal.* **2018**, *8*, 7598-7607.

- 1
2
3
4 46. Avenier, P.; Taoufik, M.; Lesage, A.; Solans-Monfort, X.; Baudouin, A.; de Mallmann,
5 A.; Veyre, L.; Basset, J. M.; Eisenstein, O.; Emsley, L.; Quadrelli, E. A. *Science* **2007**, 317,
6 1056-1060.
7 47. Chen, Y. S.; Fierro, J. L. G.; Tanaka, T.; Wachs, I. E. *J. Phys. Chem. B* **2003**, 107, 5243-
8 5250.
9 48. Visinescu, C. M.; Sanjines, R.; Lévy, F.; Marcu, V.; Pârvulescu, V. I. *J. Photochem.*
10 *Photobiol. A: Chem.* **2005**, 174, (2), 106-112.
11 49. Baiju, K. V.; Shajesh, P.; Wunderlich, W.; Mukundan, P.; Kumar, S. R.; Warriar, K. G.
12 K. *J. Mol. Catal. A* **2007**, 276, (1), 41-46.
13 50. Feng, X.; Shankar, K.; Paulose, M.; Grimes, C. A. *Angew. Chem. Int. Ed.* **2009**, 48, (43),
14 8095-8098.
15 51. Iglesia, E. *Appl. Catal. A: Gen.* **1997**, 161, (1-2), 59-78.
16 52. Liang, Y. T.; Vijayan, B. K.; Lyandres, O.; Gray, K. A.; Hersam, M. C. *J. Phys. Chem. Lett.*
17 **2012**, 3, (13), 1760-1765.
18 53. Södergren, S.; Siegbahn, H.; Rensmo, H.; Lindström, H.; Hagfeldt, A.; Lindquist, S.-
19 E. *J. Phys. Chem. B* **1997**, 101, (16), 3087-3090.
20 54. Morlanés, N.; Notestein, J. M. *J. Catal.* **2010**, 275, (2), 191-201.
21 55. Masuda, Y.; Wakamatsu, S.; Koumoto, K. *J. Eur. Ceram. Soc.* **2004**, 24, (2), 301-307.
22 56. Liu, J.; Yang, H.; Tan, W.; Zhou, X.; Lin, Y. *Electrochim. Acta* **2010**, 56, (1), 396-400.
23 57. Liu, X.; Wu, X.; Scott, K. *Catal. Sci. Technol.* **2014**, 4, (11), 3891-3898.
24 58. Chen, Y.; Fierro, J. L.; Tanaka, T.; Wachs, I. E. *J. Phys. Chem. B* **2003**, 107, (22), 5243-
25 5250.
26 59. Takahara, Y.; Kondo, J. N.; Takata, T.; Lu, D.; Domen, K. *Chem. Mater.* **2001**, 13, (4),
27 1194-1199.
28 60. Yang, M.; Allard, L. F.; Flytzani-Stephanopoulos, M. *J. Am. Chem. Soc.* **2013**, 135,
29 (10), 3768-3771.
30
31
32
33
34
35
36
37
38

Table of Contents Artwork

